Rheologically-Tailored, High-Concentration Gold Nanoparticle Pastes for Advanced Deposition-Based Sensor Manufacturing

Aleksnadra Motyka *, Sławomir Drozdek, Nina Szczotka, Iwona Grądzka-Kurzaj, Krzysztof Kubica, Aneta Wiatrowska, Karol Malecha *

Posted Date: 15 April 2026

doi: 10.20944/preprints202604.1028.v1

Keywords: gold nanoparticles; ultra-precise dispensing technology; gold microsensors and fractals

 doi:10.20944/preprints202604.1028.v1

Article

Rheologically-Tailored, High-Concentration Gold Nanoparticle Pastes for Advanced Deposition-Based Sensor Manufacturing

Aleksandra Motyka [1,2,*], Sławomir Drozdek [1,3], Nina Szczotka [1,4], Iwona Grądzka-Kurzaj [1], Krzysztof Kubica [1], Aneta Wiatrowska [1] and Karol Malecha [4,*]

[1] XTPL SA, Legnicka 48E, 54-202, Wrocław, Poland;

[2] Institute of Low Temperature and Structure Research, Polish Academy of Sciences, Okólna 2, 50-422 Wrocław, Poland;

[3] Department of Physical and Quantum Chemistry, Faculty of Chemistry, Wroclaw University of Science and Technology, Wybrzeze Wyspianskiego 27, 50-370 Wroclaw, Poland

[4] Department of Microsystems, Faculty of Electronics, Photonics and Microsystems, Wrocław University of Science and Technology, wyb. S. Wyspiańskiego 27, 50-370, Wrocław, Poland

* Correspondence: aleksandra.motyka@xtpl.com (A.M.); karol.malecha@pwr.edu.pl (K.M.)

Abstract

There is a growing demand for extreme miniaturization and enhanced sensitivity in the next-generation sensing systems, including wearable devices and bioelectronics. Such advanced platforms require highly conductive, biocompatible, and mechanically robust architectures capable of conforming to dynamic surfaces. Conventional metallic thin-film fabrication techniques have reached their fundamental physicochemical limits, often suffering from suboptimal mechanical strength, complex multi-step processing, and high costs. In contrast, additive manufacturing methodologies offer streamlined microfabrication, yet traditional printing methods frequently struggle with low-viscosity constraints, insufficient metal loading and significant material losses. Herein, the morphological fidelity, mechanical resilience, and electrical performance of the rheologically-tailored, high concentration (above 90%) gold nanoparticle paste deposited via the unique Ultra-Precise Dispensing (UPD) technology developed and continuously advanced by XTPL are assessed. The capability of the UPD system to print complex, high-density fractal geometries with linewidths down to 7 μm is evaluated on both rigid and flexible substrates, glass and polyimide, respectively. The mechanical structural integrity of these conductive traces is characterized under 360-degree bending tests. Finally, the electrical stability and thermal response of a printed proof-of-concept temperature sensor are evaluated. The printed fractal microstructures maintain excellent mechanical adhesion without cracking or delamination under severe strain, and the fabricated sensor demonstrates a highly stable, linear thermal response with a temperature coefficient of resistance of $1.98 \cdot 10^{-3}\ ^{o}C^{-1}$, validating this combined material-deposition approach for microelectronics.

Keywords: gold nanoparticles; ultra-precise dispensing technology; gold microsensors and fractals

1. Introduction

The contemporary digital economy paradigm is intrinsically linked to an ubiquitous data acquisition network facilitated by a myriad of sensing systems, ranging from wearable devices, and Integrated Industry 4.0 manufacturing lines to remote environmental monitoring platforms. Market forecasts indicate that the global sensor sector has entered a phase of exponential growth, driven by advancements in the Internet of Things (IoT), point-of-care medical diagnostics, and quantum metrology [1].

 doi:10.20944/preprints202604.1028.v1

However, as devices trend towards extreme miniaturization and enhanced detection limits, engineering faces a fundamental material-centric bottleneck that cannot be circumvented through signal processing optimization alone. Gold occupies a central position in addressing these challenges. Owing to its unique physicochemical properties - notably high electrical conductivity, exceptional chemical inertness in corrosive environments, and inherent biocompatibility - gold has emerged as a critical functional substrate in the architecture of next-generation sensing technologies.

A review of the current state-of-the-art in important applications such as Resistance Temperature Detectors (RTDs) [2–5], self-assembled monolayer/surface plasmon resonance (SAM/SPR), biosensing platforms [6–10], Surface-Enhaced Raman Spectroscopy (SERS) [11–15], and strain sensors indicates that conventional metallic thin-film fabrication techniques have reached their fundamental physicochemical limits. Depending on the specific application and fabrication technique, several critical limitations of gold-based materials must be addressed. These include susceptibility to contamination and corrosion, suboptimal mechanical strength of the resulting interconnects, and the inherent difficulty of removing stabilizing agents. Furthermore, challenges such as poor adhesion of the deposited layers, the toxicity of constituent components, and detrimental impact of surfactants/additives on overall conductivity remain significant hurdles in material optimization.

To circumvent these constraints, the integration of gold nanoparticles (AuNPs) via advanced deposition methodologies, such as Ultra-Precise Dispensing (UPD) has emerged as a pivotal technological frontier. The utilization of high-concentration (above 90% (w/w)) Au-nanoparticle-based pastes within the UPD framework enables precise architectural control over the active sensing layers, directly addressing critical challenges related to interfacial adhesion, signal reproducibility, and long-term structural stability in next-generation sensing devices. The aforementioned additive manufacturing technique facilitates a significant enhancement in both mechanical integrity and chemical purity, while streamlining the sensor fabrication process. By optimizing the architecture of the active layers, this approach ensures superior electrical stability and heightened sensitivity. Beyond general microelectronics, this architectural control is particularly crucial for electrochemical and capacitive biosensing platforms. In these specific applications, maximizing the probe density per unit area is vital. The nanostructured morphology of the paste intrinsically enhances the effective electroactive surface area (ESA), thereby facilitating the immobilization of a higher density of capture molecules (e.g., DNA) compared to planar layers deposited via conventional thin-film techniques [7,10,11].

The Au90 nanopaste formulation has been specifically engineered for the UPD process, exhibiting high viscosity and a high metallic packing fraction post-sintering. Comprehensive rheological characterization, including yield stress, thixotropic behavior, storage modulus (G’), and loss modulus (G”), was performed to establish the linear viscoelastic region (LVR). These optimized parameters ensure high material stability both pre- and post-deposition. Consequently, this approach addresses a persistent challenge in gold electrode fabrication: achieving robust interfacial adhesion. Furthermore, the high metal-loading concentration effectively mitigates the adverse effects of substrate surface roughness on the structural integrity of the deposited films. Owing to its optimized rheological and physicochemical properties, the developed Au90 nanopaste demonstrates versatile applicability, enabling its utilization in alternative deposition techniques and across a diverse range of industrial requirements. The unique structural hierarchy and surface energy profile of the synthesized gold nanoparticles in paste enable versatile post-deposition processing, facilitating consolidation not only through conventional thermal annealing but also via advanced non-thermal physical sintering mechanisms. This multi-modal sintering capability-including photonic, plasma, or electrical triggering-circumvents the thermal budget constraints of sensitive organic substrates, providing a universal platform for high-performance flexible electronics.

A significant advantage of the proposed material lies in the utilization of nanoparticles synthesized via novel, additive reductant-free protocol (main chemical additive approved by U.S. Food and Drug Administration (FDA)). By optimizing kinetic parameters - specifically through the

 doi:10.20944/preprints202604.1028.v1

precise control of the nucleation-to-growth ratio via the strategic selection of ligands and stabilizers - a robust synthesis method for pseudo-spherical nanoparticles has been established. The resulting colloidal system exhibits long-term stability (up to six months in the printing cartridge, not only in the syringe), facilitating its versatile application across a wide range of nanomaterial systems. Gold nanoparticles synthesized via the newly developed method facilitate rapid material transfer and integration with diverse deposition technologies e.g. direct writing, laser deposition. Furthermore, this approach ensures the availability of high-quality nanostructures specifically tailored for advanced functionalization, meeting the rigorous demands of versatile sensor architecture development.

2. Materials and Methods

2.1. Au90 nanopaste/formulation

The conductive architecture was fabricated using Au90 nanopaste material (XTPL S.A., Poland), a proprietary, high-viscosity metallic ink specifically engineered for advanced sensing applications. This nanopaste is characterized by an exceptionally high metallic loading of 90 wt% (solid content ranging between 87–93 wt.%), consisting of ultra-pure gold nanoparticles with a primary size distribution centered between 35 and 55 nm with a pseudo-spherical shape, as verified by transmission electron microscopy (TEM). Figure 1 shows the size distribution along with an illustrative electron microscope image. In contrast, Dynamic Light Scattering (DLS) measurements indicate an effective hydrodynamic diameter of 80–130 nm, suggesting the formation of stable, soft-agglomerated clusters within the organic vehicle. Table 1 summarizes the most important properties of the Au90 nanopaste material. To ensure high-resolution deposition and structural integrity, the formulation exhibits a distinct non-Newtonian rheological profile, with a dynamic viscosity exceeding 1x10^5 mPa*s at low shear rates, as shown in Figure 2. Upon thermal processing at 350°C for 20 minutes in an ambient atmosphere, the sintered tracks demonstrate excellent electrical performance, reaching a low bulk resistivity of 8.13 $\mu\Omega$*cm.

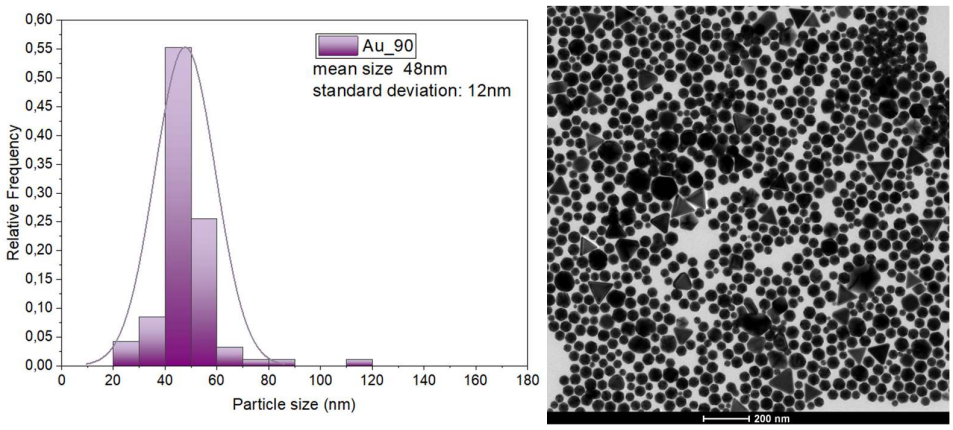

Figure 1. (Left) Size distribution and (right) illustrative TEM image of gold nanoparticles in Au90 nanopaste.

Table 1. Characteristic values for Au90 nanopaste material.

Paste	Solid content	Metal content (wt.%)	Mean nanoparticle size [nm] (TEM)	Average nanoparticle size [nm] (DLS)	Electrical resistivity [$\mu\Omega$*cm]	Viscosity (25°C) [mPa*s]
Au90 nanopaste	87-93	90	35-55	80 – 130	8.13 (350°C; 20 min; Air)	> 100 000 (Shear Rate = 0.2 s-1)

 doi:10.20944/preprints202604.1028.v1

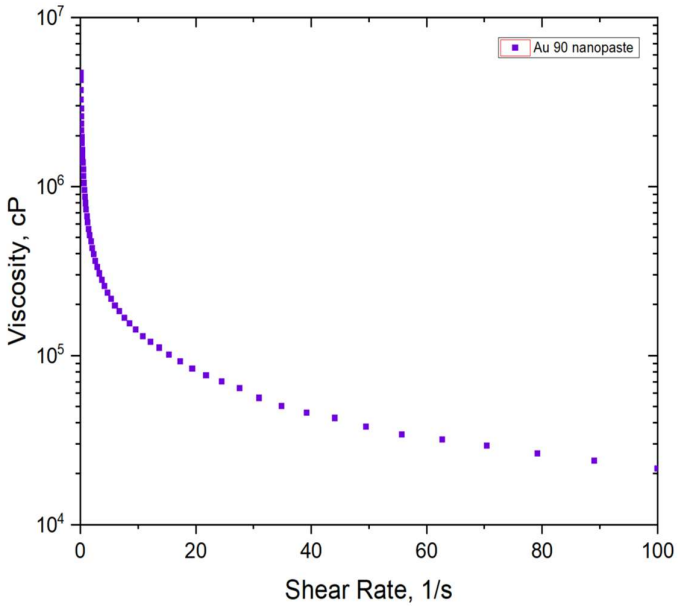

Figure 2. Viscosity as a function of the shear rate for Au90 nanopaste.

This high-viscosity framework is optimized for UPD, facilitating the formation of dense, sub-micron conductive traces with minimal thermal budget requirements. To achieve robust steric stabilization of the gold nanostructures, a novel, internally designed modification of the polyol synthesis was implemented. The resulting colloidal suspension underwent rigorous purification via controlled precipitation to eliminate residual precursors and secondary by-products. In the final stage, the material properties were precisely engineered by introducing a synergistically compatible system of organic solvents and stabilizing agents, specifically tailored to ensure long-term colloidal integrity and optimal rheological performance for the paste.

2.2. High-Density Fractal By Gold Paste Printing

These microfabrication tasks to high-density fractals were performed using the UPD technology in Delta Printing System (DPS). The Au90 nanopaste was dispensed at a controlled pressure of 3000 mbar with a translation speed of 0.20 to 0.25 mm/s. Initial results showed linewidths ranging from 7 to 13 μm on glass and 8 to 15 μm on Kapton. Following dispensing, the structures were thermal sintered on a hot-plate at 350°C for 20 minutes.

2.3. Temperature sensor

Prior to printing, the glass substrate (soda-lime glass slide 76x25x1 mm**,** Chemland, Poland) was cleaned by an initial rinse with acetone followed by demineralized water, then subjected to ultrasonic cleaning in a mixture of isobutanol and rokafenol (PCC Rokita, Poland) (80:1 ratio) for 15 min. After a subsequent flush with DI water, the slide underwent further ultrasonic cleaning in a water bath for 15 min, followed by a 20 s immersion in water at 80°C. The substrate was finally dried using compressed nitrogen.

The Au90 nanopaste was dispensed using the UPD system onto a glass slide at a pressure of 2000 mbar and a translation velocity of 1 mm/s. The opening of the nozzle was 10 μm outside diameter.

The pattern was sintered at 350°C for 20 minutes on a hotplate. The resultant line width (after sintering) varies from 15 to 18 μm, height ~1 μm.

Jumper wires were mounted to the microscope glass slide near the lines leading from the printed pattern. An electrical connection was created with solder paste T7-type NP303-DPF201-T7 (NIHON GENMA MFG. CO., LTD., Japan). The assembly was heated at 215 °C for 2 min to facilitate electrical

 doi:10.20944/preprints202604.1028.v1

bonding. The printed pattern was encapsulated using a Chemland cover glass coated with Norland Optical Adhesive 81 (NOA 81, Norland Products Inc., USA). Structural integrity was secured via photocuring for 2 min using a multi-lamp irradiation chamber equipped with four 9 W low-pressure mercury-vapor emitters (36 W total power). A secondary application of NOA 81 was applied to the solder joints and photocured for an additional 2 min to reinforce the connection points.

Resistance in time was recorded with KEYSIGHT 6 ½ Digit Multimeter. The total time interval between measurements was 600 ms. Temperature response was detected with PicoLog TC-08 high-resolution thermocouple data logger with 200 ms time interval. Type K thermocouple was mounted with a tape to the surface of the sensor device. Preliminary performance was verified by monitoring the sensor's response to thermal stimulation.

3. Results

3.1. High-Density Fractal By Gold Paste Printing

The implementation of deterministic fractal geometries through UPD technology provides a robust framework for exploring hard-soft material integration in microelectronics. In this study, we evaluated five distinct motifs - Gosper, Hilbert, Peano, Sierpinski, and a Double Spiral - to investigate their space-filling properties and mechanical adaptability. These patterns, confined to a 3 x 3 mm footprint, allow for a high packing density of conductive traces, which is essential for device miniaturization. By utilizing self-similar layouts, these structures incorporate spring-like motifs across multiple scales, offering enhanced elastic strain capabilities compared to traditional periodic serpentines [16–18]. This mechanical resilience is particularly relevant for epidermal electronics, enabling devices to conform to the curvilinear and dynamic surfaces of biological tissues [19].

The selection of these specific topologies was guided by their unique geometric and functional advantages. The Hilbert and Peano curves ensure highly uniform surface coverage, while the Gosper and Sierpinski motifs provide hierarchical connectivity that enhances robustness against localized structural defects. Furthermore, the absence of closed loops in those layouts minimizes RF-induced eddy currents, potentially offering invisibility under magnetic resonance imaging [16]. The Double Spiral motif was included to explore the feasibility of printing inductive components and antenna-like structures, building upon established fractal antenna design concepts [20].

This study focuses on the evaluation of the printing process and the characterization of the paste’s behavior during complex path dispensing. These variations reflect the process optimization and the rheological challenges associated with dispensing high-viscosity nanopastes through microscale nozzles. The results demonstrate that UPD is a promising technology for the precise fabrication of advanced conductive microstructures with high morphological fidelity on rigid glass substrates. Having established the spatial resolution limits, the subsequent phase of our study evaluated the mechanical resilience of these complex structures on flexible platforms. Figure 3 and Figure 4 show various patterns printed using the UPD technology described above.

 doi:10.20944/preprints202604.1028.v1

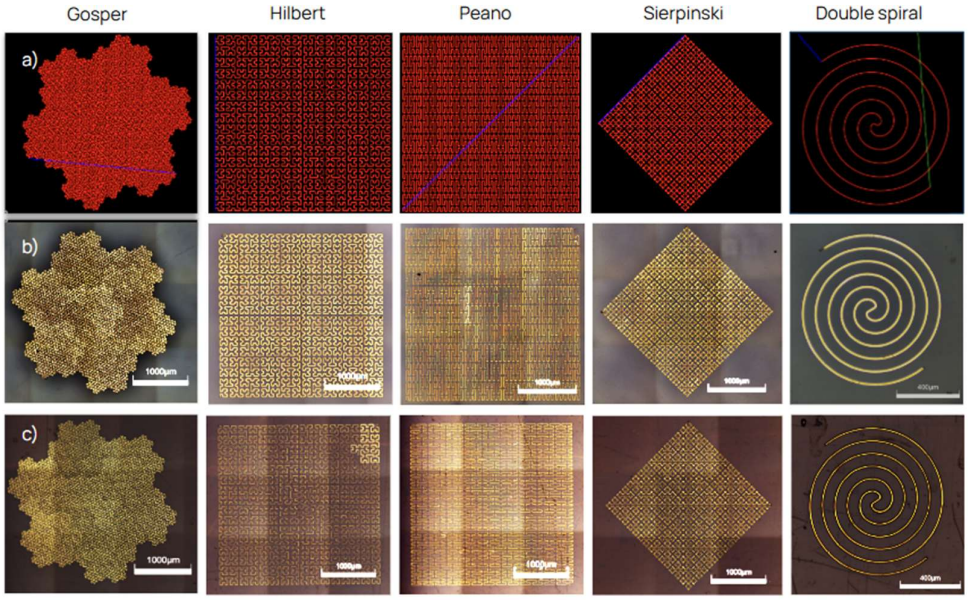

Figure 3. Fabrication and morphological characterization of fractal-based designs via UPD. (a) Digital representations of the Gosper, Hilbert, Peano, Sierpinski, and Double Spiral patterns in render mode on UPD. (b) Optical images of the gold traces printed on glass substrates (Double Spiral dimension: 1 x 1 mm; others: 3 x 3 mm). (c) Corresponding gold structures printed on flexible Kapton foil. Scale bars: 1000 µm (400 µm for Double Spiral). Samples (b) and (c) after the sintering process.

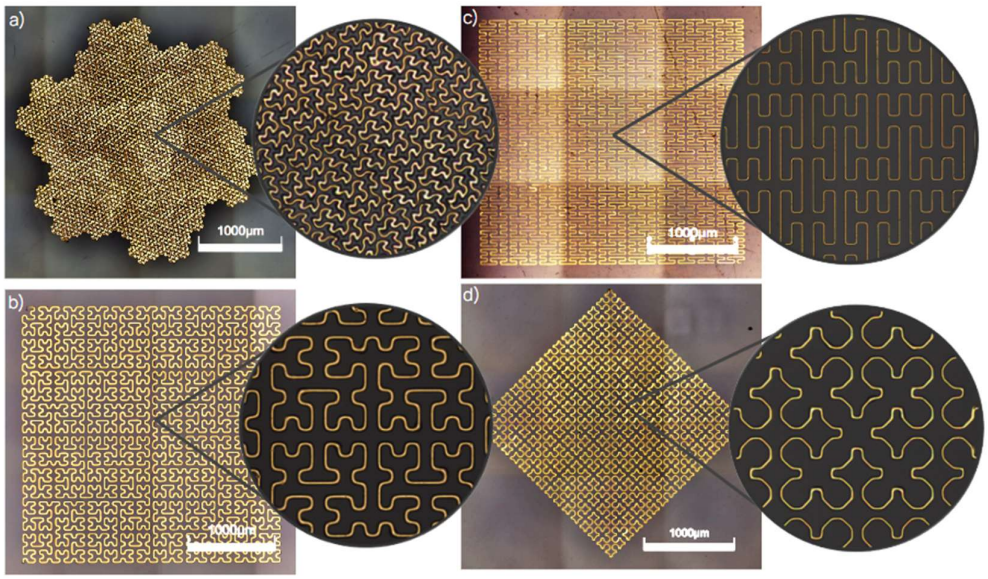

Figure 4. Optical images showing the magnified details of printed fractals using UPD technology. (a) Gosper fractal with line width 11 µm printed on glass substrate. (b) Hilbert fractal with line width 17 µm printed on glass substrate. (c) Peano fractal with line width 5 µm printed on Kapton foil. (d) Sierpinski fractal with line width 7 µm printed on glass substrate.

To assess the mechanical stability of the printed traces, 360-degree bending tests were conducted on the Kapton (DuPont) - supported samples. As shown in Figure 5, the polyimide strips were subjected to an U-shaped curvature, where the two ends of the substrate were brought together to achieve near 360-degree deformation. Optical inspection confirmed that the gold traces maintained

 doi:10.20944/preprints202604.1028.v1

structural integrity without cracking or delamination throughout the bending process. This robustness suggests that the adhesion and rheological properties of the gold nanopaste are well-suited for flexible substrates, allowing the deterministic fractal motifs to effectively dissipate mechanical stress even under severe physical strain.

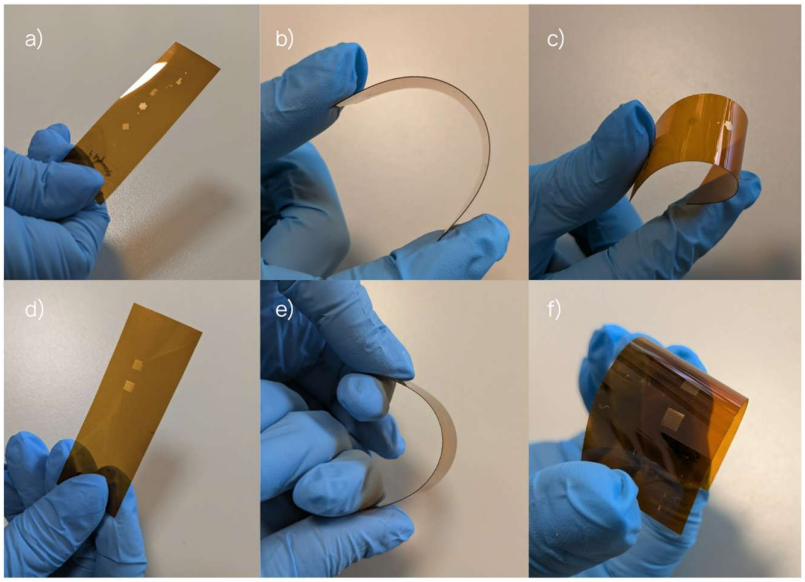

Figure 5. Mechanical reliability and bending performance of fractals on Kapton. (a,d) Flat state of printed fractal samples on polyimide strips. (b,c,e,f) Samples under manual bending, illustrating the structural integrity and macroscopic flexibility of the gold nanopaste traces.

3.2. Temperature sensor

To demonstrate the practical utility of the Au90 nanopaste, a proof-of-concept temperature sensor was fabricated (as shown in Figure 6 and Figure 7), consisting of a serpentine resistor pattern with a total line length of 39.6 cm. The active area was designed to fit within a 5 mm diameter circle.

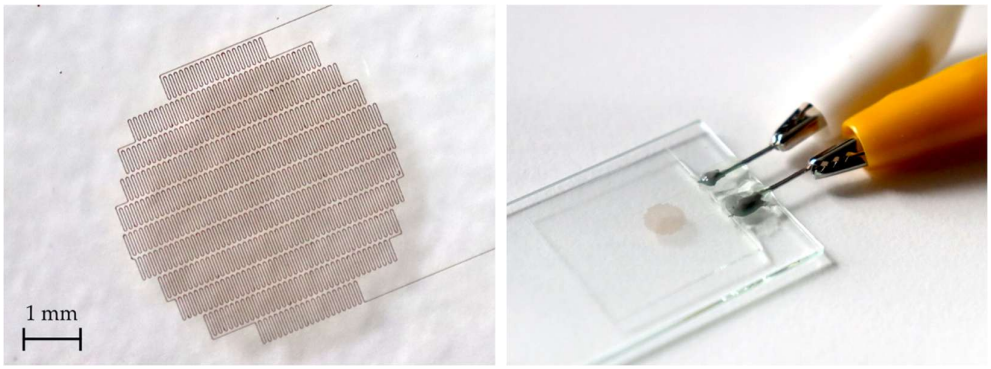

Figure 6. Photographs of the printed temperature sensor. (Left) detailed view of the active area and (right) photograph of the device connected for characterization.

 doi:10.20944/preprints202604.1028.v1

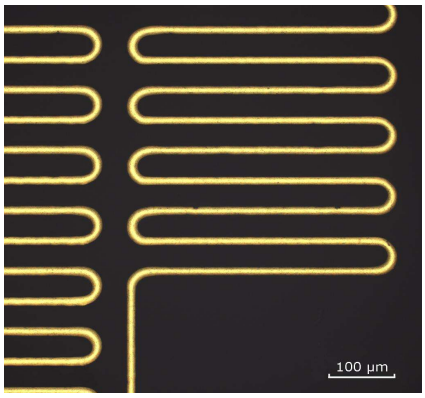

Figure 7. High-magnification optical image of the sensor track. Scale bar: 100 µm .

Figure 8 A illustrates the rapid resistance change upon contact with a pre-heated fingertip. There is a clear resistance response for the change of the temperature. The temperature dependence of the resistance was further characterized within the relaxation interval of 25–90s (Figure 8B), providing the basis for subsequent calculations. The intercept of the linear regression analysis indicates an R_0 value of 2807.5 +/- 0.3 Ω at 0°C.

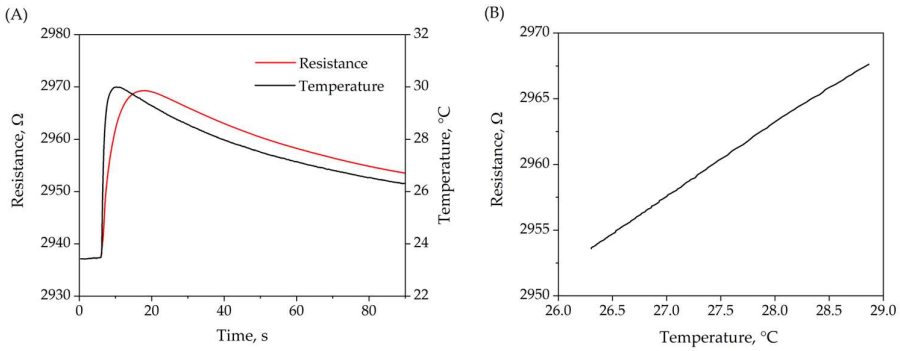

Figure 8. (A) Transient resistance and temperature measurements of the gold sensor over the duration of the heating experiment. (B) Ohmic response as a function of temperature.

4. Discussion

The logic behind choosing fractal geometries for this study, as opposed to standard Euclidean shapes: such as solid rectangles or simple grids, is rooted in their extraordinary space-filling properties and unique mechanical behavior. Fractals are defined by mathematical iterations that produce self-similar patterns—where the structural geometry remains consistent across multiple length scales. This property represents an engineering breakthrough for miniaturization; as demonstrated by Herbko and Łopato [21], such designs allow for a four-fold reduction in sensor area with only a two-fold decrease in sensitivity, a trade-off that is unachievable with traditional planar electrodes. Further research by Herbko et al. [22] suggests that transitioning to fractal resonators can result in a footprint reduction of up to 80% without shifting the operational frequency. In our work, we pushed these boundaries even further by utilizing exceptionally high iteration orders: the 6th order for the Hilbert curve and the 4th order for the Peano curve. The resulting complexity, consisting of thousands of individual vector segments, reached the computational limits of standard CAD environments, highlighting the significant processing task managed by the UPD platform during real-time trajectory execution.

From a process engineering standpoint, the technical simplicity and "one-step" nature of UPD technology offer a decisive advantage over other additive and subtractive methods. Conventional

 doi:10.20944/preprints202604.1028.v1

cleanroom microfabrication (CVD/PVD combined with photolithography) is notoriously laborious, requiring expensive masks, hazardous etchants, and capital investments often exceeding USD 1 million [23]. While Aerosol Jet Printing serves as a maskless alternative, it frequently suffers from "overspray" and requires complex sheath gas management to maintain focus. Traditional Inkjet Printing is further limited by the necessity for very low-viscosity inks, which typically have low metal loading and require multiple layers to achieve functional conductivity [19,23]. In contrast, our UPD approach utilizes an Au90 nanopaste with 90 wt.% metal content. This allows for the deposition of dense, high-aspect-ratio traces in a single pass. Although UPD technology is capable of reaching a resolution of 1 μm, we deliberately utilized linewidths of 7–13 μm in this study as a strategic engineering trade-off to ensure maximum process yield and line continuity across the most intricate sections, such as the rapid directional changes in the Gosper curve.

The Gosper curve (5th order) served as the ultimate "stress test" for the UPD system's stability. Due to its high density of sharp turns and the need for constant, rapid changes in the printing head's trajectory, it represents the most demanding scenario for high-viscosity dispensing. The successful printing of a continuous 11 μm line on glass and 9 μm on Kapton for this motif confirms that the DPS system's pneumatic control and trajectory execution can handle extreme geometric complexity without nozzle clogging or flow interruption. Mechanically, the 360-degree bending tests on the Kapton substrate proved the superiority of the "structure that stretches" strategy. By replacing sharp mathematical vertices with arc sections, we effectively neutralized stress concentration points that typically lead to cracking, while also stabilizing the electrical response of the patterns [24]. During deformation, the fractal units exhibit an in-plane rotation—a mechanism likened by Ho et al. [25] to the "motion of scissors"—which dissipates strain and allows the gold traces to endure stresses far beyond the 20% elastic limit of biological tissue [19,25,26].

The selection of gold as the primary material was dictated by its biocompatibility and chemical inertness, which is critical for future biosensors exposed to sweat and environmental moisture. As noted by Zamani et al. [23], gold electrodes with high surface areas and rougher morphologies enhance charge transfer and reduce steric hindrance for bio-functionalization. Functionally, these architectures act as geometric signal amplifiers. The extreme density of vertices triggers a phenomenon known as the lightning rod effect, creating localized regions of high electric field intensity "*hot-spots*" that significantly increase the capacitive response of the sensors [18]. This enhancement is even more pronounced at higher iteration orders, as confirmed by recent studies on meta-absorbers [27]. By achieving resolutions in the 7–15 μm range, we provide a platform where device performance can be precisely "tuned" by increasing the fractal order—more edges lead to better charge accumulation on the same minimal surface area [18,22]. Furthermore, the absence of closed loops in these specific layouts (e.g., Hilbert, Peano) ensures MRI-compatibility by eliminating RF-induced eddy currents [16]. This work confirms that UPD-printed gold fractals bridge the gap between high-end lithography and scalable additive manufacturing, aligning with the principles of rational design for next-generation bio-materials. To fully contextualize the performance of the proposed Au90 nanopaste/UPD approach, a comparative analysis against current state-of-art additive manufacturing techniques is presented in Table 2. As demonstrated, the UPD method uniquely combines ultra-fine resolution (<10 μm) with exceptionally high metal loading, maintaining excellent mechanical flexibility. While traditional inkjet and aerosol jet printing methods typically rely on low-viscosity inks with metal contents ranging from 5 to 25 wt.%, the Au90 nanopaste successfully utilizes a highly viscous (above 100 000 mPas) formulation without sacrificing print resolution. In fact, it achieves a highly competitive minimum linewidth of 7-8 μm, which surpasses the resolution of standard inkjet printing (<20 μm to 95 μm) and bridges the gap toward complex directed self-assembly methods. Furthermore, despite the massive metal concentration, the sintered structures maintain excellent mechanical flexibility, withstanding 360-degree bending on Kapton substrate, which is often a challenge for highly loaded conductive traces. Summarizing, this unique combination of ultra-fine resolution, maximized conductive mass in a single pass, and robust

 doi:10.20944/preprints202604.1028.v1

mechanical resilience positions the UPD-printed Au90 nanopaste as a superior and highly scalable candidate for next-generation, miniaturized flexible electronics and biosensors.

Table 2. Comparison of rheological, morphological, and electro-mechanical properties of AuNPs based formulations across advanced additive deposition methods.

Printing method	Material	Viscosity (mPa·s)	Metal content (wt.%)	Min. linewidth (μm)	TCR (10^{-3} °C^{-1})	Mechanical Flexibility/Strain	Ref.
Ultra-Precise Dispensing	Au90 nanopaste	> 100 000	>90	7-8	1.98	High (360 bending on Kapton)	[This work]
Inkjet Printing	PVP-stabilized Au NPs suspended in a mixture of H_2O, EtOH, and EG	1-16	5	~100	Not investigated	High (prints were successfully tested on very thin and flexible substrates	[28]
Aerosol Jet Printing	PVP-stabilized Au NPs suspended in a mixture of H_2O, EtOH, and EG	1-16	5	15-20	Not investigated	High (prints were successfully tested on very thin and flexible substrates	[28]
Inkjet Printing	Octanethiol-functionalized Au NPs (OT-AuNPs) with a TrisSH dispersed in terpineol	-	25	~95±5	Not investigated	Very High (stability confirmed over 1000 bending cycles at a radius of r = 0.6 cm)	[29]
Drop-on-Demand Inkjet Printing	Au NP ink JG-125 (commercial)	-	-	35 (drop spacing)	2.7	Rigid (tested on alumina ceramic substrates for airborne equipment)	[30]
Inkjet Printing	PVP-capped AuNPs in H_2O/Diethylene glycol/glycerol mixtures	-	11	20	Not investigated	Rigid (printed on soda lime glass)	[31]
Inkjet Printing	Aqueous AuNPs capped with PVP40	2.5-5.8	0.03-0.12	-	Not investigated	High (good wettability and continuous patterns on flexible photo paper)	[32]
Inkjet Printing	AuNPs protected by PVP and acrylic resin in H_2O and EtOH	~1-3	20	100	Not investigated	High (printed successfully on silicon, glass, paper, and flexible projection film)	[33]
Directed Self-Assembly/ Bar coating	π-junction AuNP ink	-	15-25	0.6	Not investigated	High (fabricated on flexible cyclic olefin polymer substrates)	[34]
Flexographic Printing	PVP-capped AuNPs dispersed in 70% IPA/30% H_2O	-	-	100-120	Not investigated	High (printed on flexible polyimide substrates)	[35]
Inkjet Printing	1. AuNP ink: 35% wt. AuNP solution, 55% wt. glycerol, 10% wt. propan-2-ol; 2. Precursor ink: $HAuCl_4$ in 20% wt. H_2O, 70% wt. ethylene glycol, 10% wt. Propan-2-ol	11.2 for 1st formulation 14.0 for 2nd formulation	5 for 1st formulation 20 for 2nd formulation	~37	Not investigated	High (successfully printed and evaluated on 50 um thick flexible polyimide foil)	[36]
Plasma Jet Printing	PVP-stabilized AuNPs synthesized via USP and redispersed in EtOH	~50-70	0.025	550	Not investigated	Rigid (printed on Al_2O_3 technical ceramic substrates)	[37]
Inkjet Printing	AuNPs stabilized in sugar-based	1.9-2.1	1.5-3.0	35	Not investigated	High (printed on premium glossy photo paper)	[38]

 doi:10.20944/preprints202604.1028.v1

	biodegradable comb-like polyurethane polymer-matrix

Beyond the structural and mechanical advantages of the fractal designs, the intrinsic electrical reliability of the sintered Au90 nanopaste was validated through the fabrication of a functional prototype device.

The electrical performance of the prototype temperature sensor exhibited a robust metallic character within the analyzed temperature range and high sensitivity to thermal fluctuations. A non-linear relationship between resistance and temperature was observed during the initial transient heating phase, attributed to the thermal lag induced by the encapsulation layer. During this period, the system is in a non-equilibrium state where a temperature gradient exists between the external reference and the embedded Au90 nanopaste lines of the sensor. However, in the subsequent relaxation region (25 s - 90 s from the measurement start) the system approaches thermal equilibrium. Strong linear dependency between the relative change in resistance ($\Delta R/R_0$, where $\Delta R = R - R_0$) and temperature (Figure 9) was found for it with a near-unity correlation. The Temperature Coefficient of Resistance (TCR) was extracted from the slope. The resulting TCR for the sensor was determined to be (1.9800 +/- 0.0039)*10^{-3} $°C^{-1}$. This value represents a notably high performance relative to the previously reported inkjet-printed temperature sensors in the literature [10]. While TCR is approximately 57% of the value for bulk gold (3.5 x 10^{-3} $°C^{-1}$) [39]. However, the deviation is typical for printed structures due to grain boundaries, porosities or organic stabilizers that can remain after sintering [39,40].

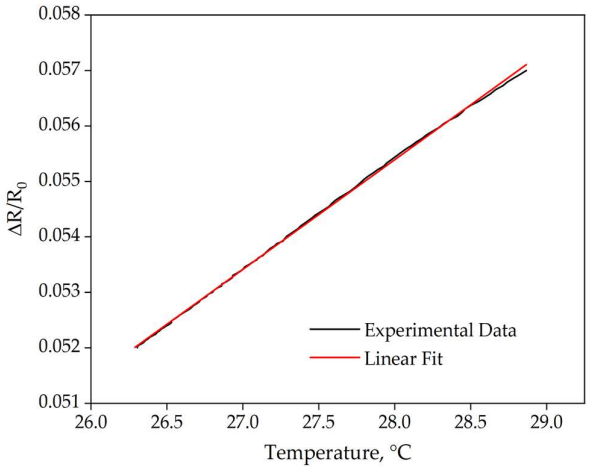

Figure 9. Normalized resistance ΔR/R as a function of temperature. The slope of the linear fit (red line) represents the temperature coefficient of resistance (TCR).

Owing to its simplified architecture and cost-effective fabrication process in this case, the proposed sensor serves as an ideal functional foundation for the advancement of next-generation wearable electronics and flexible monitoring systems.

Building upon these promising results, future work will focus on derivative ink formulations, based on the aforementioned gold nanostructures. These are currently being developed and validated for compatibility with alternative deposition methods, such as Laser-Induced Forward Transfer (LIFT) technology within the framework of the European ULTRA-SOUND with Bioimpedance Analysis and Graphene FET-enhanced Wearable Sensing For Decentral Health-monitoring project (HORIZON-CL4-2023-RESILIENCE-01-33). This endeavor aims to introduce a novel concept of a stretchable multi-sensing platform for advanced wearable body composition analysis.

 doi:10.20944/preprints202604.1028.v1

5. Conclusions

We report on a high-concentration gold nanoparticle (AuNP) architecture, synthesized via a refined polyol-mediated route, exhibiting bespoke rheological properties designed to bridge the gap between laboratory synthesis and industrial-scale integration. This material paradigm addresses the critical bottlenecks currently hindering the evolution of electronic and bioelectronic sensing platforms. When coupled with the XTPL UPD system, this framework enables the fabrication of electrodes with unprecedented feature resolution, facilitating extreme miniaturization across a diverse range of substrate geometries. Furthermore, the inherent versatility of this green-chemistry-based synthesis allows for precise iterative tuning to ensure compatibility with established microelectronic deposition standards. These high-purity AuNPs not only serve a robust sensing transducers but also provide a pristine scaffold for advanced molecular functionalization, offering a sustainable and scalable pathway for next-generation sensor development.

Author Contributions: "Conceptualization, A.M.; printing methodology, N. Sz.; sensor proof-of-concept, I.G.-K.; formal analysis, A.M. and S.D.; resources, A.M. and S.D.; data curation, I.G.-K and K.K.; writing—original draft preparation, A.M..; writing—review and editing, A.M. and S.D..; supervision, K.M. and A.W.; All authors have read and agreed to the published version of the manuscript."

Conflicts of Interest: The authors declare no conflicts of interest.

Abbreviations

The following abbreviations are used in this manuscript:

UPD	Ultra-Precise Dispensing
IoT	Internet of Things
RTDs	Resistance Temperature Detectors
SAM	Self-Assembled Monolayer
SPR	Surface Plasmon Resonance
SERS	Surface-Enhaced Raman Spectroscopy
Au NPs	Gold nanoparticles
ESA	Electroactive Surface Area
LVR	Linear viscoelastic region
FDA	Food and Drug Administration
XTPL S.A.	XTPL Spolka Akcyjna
TEM	Transmission Electron Microscopy
DLS	Direct Light Scattering
CVD	Chemical Vapor Deposition
PVD	Physical Vapor Deposition
TCR	Temperature Coefficient of Resistance
G-FET	Graphene Field Effect Transistors
RF	Radio Frequency
LIFT	Laser Induced Forward Transfer

References

1. Butt, M.A. Thin-Film Sensors for Industry 4.0: Photonic, Functional, and Hybrid Photonic-Functional Approaches to Industrial Monitoring. *Coatings* **2026**, *16*, 93, doi:10.3390/coatings16010093.

 doi:10.20944/preprints202604.1028.v1

2. Lee, Y.; Lee, Y.S. A New Submersion Detection Sensor Using Two Resistance Temperature Detectors Operating on the Thermal Equilibrium Principle. *Sensors* **2019**, *19*, 4310, doi:10.3390/s19194310.
3. Sarma, S.; Lee, J.H. Developing Efficient Thin Film Temperature Sensors Utilizing Layered Carbon Nanotube Films. *Sensors* **2018**, *18*, 3182, doi:10.3390/s18103182.
4. Aliazizi, F.; Özsoylu, D.; Bakhshi Sichani, S.; Khorshid, M.; Glorieux, C.; Robbens, J.; Schöning, M.J.; Wagner, P. Development and Calibration of a Microfluidic, Chip-Based Sensor System for Monitoring the Physical Properties of Water Samples in Aquacultures. *Micromachines* **2024**, *15*, 755, doi:10.3390/mi15060755.
5. Lugoda, P.; Costa, J.C.; Oliveira, C.; Garcia-Garcia, L.A.; Wickramasinghe, S.D.; Pouryazdan, A.; Roggen, D.; Dias, T.; Münzenrieder, N. Flexible Temperature Sensor Integration into E-Textiles Using Different Industrial Yarn Fabrication Processes. *Sensors* **2019**, *20*, 73, doi:10.3390/s20010073.
6. Sakellari, G.I.; Hondow, N.; Gardiner, P.H.E. Factors Influencing the Surface Functionalization of Citrate Stabilized Gold Nanoparticles with Cysteamine, 3-Mercaptopropionic Acid or l-Selenocystine for Sensor Applications. *Chemosensors* **2020**, *8*, 80, doi:10.3390/chemosensors8030080.
7. Mahadhy, A.; Mattiasson, B.; StåhlWernersson, E.; Hedström, M. Evaluation of Polytyramine Film and 6-Mercaptohexanol Self-Assembled Monolayers as the Immobilization Layers for a Capacitive DNA Sensor Chip: A Comparison. *Sensors* **2021**, *21*, 8149, doi:10.3390/s21238149.
8. Cennamo, N.; Chiavaioli, F.; Trono, C.; Tombelli, S.; Giannetti, A.; Baldini, F.; Zeni, L. A Complete Optical Sensor System Based on a POF-SPR Platform and a Thermo-Stabilized Flow Cell for Biochemical Applications. *Sensors* **2016**, *16*, 196, doi:10.3390/s16020196.
9. Zhang, H.; Gao, Z.; Zhang, Y.; Hou, R.; Zhang, H.; Yan, Z.; Tian, J.; Tao, P.; Zhou, X. Research Progress on Nanomaterials in SPR Sensors. *Nanomaterials* **2025**, *15*, 1847, doi:10.3390/nano15241847.
10. Masdor, N.; Altintas, Z.; Tothill, I. Surface Plasmon Resonance Immunosensor for the Detection of Campylobacter Jejuni. *Chemosensors* **2017**, *5*, 16, doi:10.3390/chemosensors5020016.
11. Das, G.M.; Managò, S.; Mangini, M.; De Luca, A.C. Biosensing Using SERS Active Gold Nanostructures. *Nanomaterials* **2021**, *11*, 2679, doi:10.3390/nano11102679.
12. Pollap, A.; Świt, P. Recent Advances in Sandwich SERS Immunosensors for Cancer Detection. *Int. J. Mol. Sci.* **2022**, *23*, 4740, doi:10.3390/ijms23094740.
13. Hwang, J.; Yang, M. Sensitive and Reproducible Gold SERS Sensor Based on Interference Lithography and Electrophoretic Deposition. *Sensors* **2018**, *18*, 4076, doi:10.3390/s18114076.
14. Zhou, H.; Li, D.; Lee, C. Technology Landscape Review of In-Sensor Photonic Intelligence: From Optical Sensors to Smart Devices. *AI Sens.* **2025**, *1*, 5, doi:10.3390/aisens1010005.
15. Khonina, S.N.; Kazanskiy, N.L. Trends and Advances in Wearable Plasmonic Sensors Utilizing Surface-Enhanced Raman Spectroscopy (SERS): A Comprehensive Review. *Sensors* **2025**, *25*, 1367, doi:10.3390/s25051367.
16. Fan, J.A.; Yeo, W.-H.; Su, Y.; Hattori, Y.; Lee, W.; Jung, S.-Y.; Zhang, Y.; Liu, Z.; Cheng, H.; Falgout, L.; et al. Fractal Design Concepts for Stretchable Electronics. *Nat. Commun.* **2014**, *5*, 3266, doi:10.1038/ncomms4266.
17. Szczotka, N.; Motyka, A.; Chudzyńska, A.; Łysień, M.; Perczyńska, A.; Szczurek, A.; Witczak, Ł.; Kowalczewski, P.; Wiatrowska, A. Ultra-Precise Dispensing in 3D Packaging: A Seamless Shift from R&D to Production. *IMAPSource Proc.* **2025**, *2024*, doi:10.4071/001c.129769.
18. Novakovic, Z.; Dubourg, G.; Joksović, S.; Stanojev, J.; Djuric, N.M.; Djuric, S.M. Fractal-Electrodes Designed with ZnO Nano-Pebble Film for Sensitive and Stable Capacitive Humidity Sensing in Wearable Applications. *Sens. Actuators Phys.* **2025**, *396*, 117211, doi:10.1016/j.sna.2025.117211.
19. Kim, D.-H.; Lu, N.; Ma, R.; Kim, Y.-S.; Kim, R.-H.; Wang, S.; Wu, J.; Won, S.; Tao, H.; Islam, A.; et al. Epidermal Electronics. *Science* **2011**, *333*, 838–843, doi:10.1126/science.1206157.
20. Cohen N. Communications Quarterly. In *Fractal antennas: Part 1*; 1995; pp. 7–22.
21. Herbko, M.; Lopato, P. Microstrip Patch Strain Sensor Miniaturization Using Sierpinski Curve Fractal Geometry. *Sensors* **2019**, *19*, 3989, doi:10.3390/s19183989.
22. Herbko, M.; Lopato, P.; Psuj, G.; Rajagopal, P. Application of Selected Fractal Geometry Resonators in Microstrip Strain Sensors. *IEEE Sens. J.* **2022**, *22*, 12656–12663, doi:10.1109/JSEN.2022.3177932.
23. Zamani, M.; Klapperich, C.M.; Furst, A.L. Recent Advances in Gold Electrode Fabrication for Low-Resource Setting Biosensing. *Lab. Chip* **2023**, *23*, 1410–1419, doi:10.1039/D2LC00552B.

 doi:10.20944/preprints202604.1028.v1

24. Dihan Hasan and Chengkuo Lee A Modified Abstraction of Sierpiński Fractals towards Enhanced Sensitivity of a Cross-Coupled Bow-Tie Nanostructure. **2018**.
25. Ho, M.D.; Liu, Y.; Dong, D.; Zhao, Y.; Cheng, W. Fractal Gold Nanoframework for Highly Stretchable Transparent Strain-Insensitive Conductors. *Nano Lett.* **2018**, *18*, 3593–3599, doi:10.1021/acs.nanolett.8b00694.
26. Wang, H.; Yang, Y.; Zhou, X.; Tian, J.; Duan, X.; Li, A.; Lu, T.J.; Li, X.; Pei, D.; Xu, F. Rational Design of Mechanical Bio-Metamaterials for Biomedical Applications. *Prog. Mater. Sci.* **2026**, *156*, 101545, doi:10.1016/j.pmatsci.2025.101545.
27. Islam, F. Sierpinski-Fractal Inspired Ultra-Broadband UV-NIR Meta Absorber: Notable Impact on the Self-Stabilization of Light-Sail or Solar-Sail. **2024**.
28. Valayil Varghese, T.; Eixenberger, J.; Rajabi-Kouchi, F.; Lazouskaya, M.; Francis, C.; Burgoyne, H.; Wada, K.; Subbaraman, H.; Estrada, D. Multijet Gold Nanoparticle Inks for Additive Manufacturing of Printed and Wearable Electronics. *ACS Mater. Au* **2024**, *4*, 65–73, doi:10.1021/acsmaterialsau.3c00058.
29. Im, J.; Trindade, G.F.; Quach, T.T.; Sohaib, A.; Wang, F.; Austin, J.; Turyanska, L.; Roberts, C.J.; Wildman, R.; Hague, R.; et al. Functionalized Gold Nanoparticles with a Cohesion Enhancer for Robust Flexible Electrodes. *ACS Appl. Nano Mater.* **2022**, *5*, 6708–6716, doi:10.1021/acsanm.2c00742.
30. Acosta, C.; Flynn, W.P.; Santillan, L.; Garnsey, S.; Bhalla, A.S.; Guo, R. The Performance Characterization of a Drop-on-Demand Inkjet-Printed Gold Film Under the Temperature Conditions for Airborne Equipment. *J. Compos. Sci.* **2025**, *9*, 231, doi:10.3390/jcs9050231.
31. Rahman, M.T.; Cramer, J.; Noor, M.I.; Rottmann, P.F.; Huckaba, A.J. Stable Gold Nanoparticle Colloids for Inkjet Printing Conductive Films. *Surf. Interface Anal.* **2025**, *57*, 729–738, doi:10.1002/sia.70006.
32. Shariq, M.; Rudolf, R.; Majerič, P.; Chattopadhyaya, S.; Kargl, R.; Friedrich, B.; Grace, A.N.; Dixit, A.R. Jettability and Printability of Customized Gold Nanoparticles-Based Ink on Flexible Substrate through Inkjet Printing Process. *Colloids Surf. Physicochem. Eng. Asp.* **2024**, *682*, 132837, doi:10.1016/j.colsurfa.2023.132837.
33. Cui, W.; Lu, W.; Zhang, Y.; Lin, G.; Wei, T.; Jiang, L. Gold Nanoparticle Ink Suitable for Electric-Conductive Pattern Fabrication Using in Ink-Jet Printing Technology. *Colloids Surf. Physicochem. Eng. Asp.* **2010**, *358*, 35–41, doi:10.1016/j.colsurfa.2010.01.023.
34. Li, L.; Li, W.; Sun, Q.; Liu, X.; Jiu, J.; Tenjimbayashi, M.; Kanehara, M.; Nakayama, T.; Minari, T. Dual Surface Architectonics for Directed Self-Assembly of Ultrahigh-Resolution Electronics. *Small* **2021**, *17*, 2101754, doi:10.1002/smll.202101754.
35. Benson, J.; Fung, C.M.; Lloyd, J.S.; Deganello, D.; Smith, N.A.; Teng, K.S. Direct Patterning of Gold Nanoparticles Using Flexographic Printing for Biosensing Applications. *Nanoscale Res. Lett.* **2015**, *10*, 127, doi:10.1186/s11671-015-0835-1.
36. Le Porcher, B.; Rieu, M.; Viricelle, J.-P. Development of Gold Inks for Inkjet Printing of Gas Sensors Electrodes on Plastic Support. *Electronics* **2024**, *13*, 2110, doi:10.3390/electronics13112110.
37. Kresnik, L.; Majerič, P.; Feizpour, D.; Rudolf, R. Development of a Gold Nanoparticle Dispersion for Plasma Jet Printing on Solid Substrates. *Materials* **2025**, *18*, 2713, doi:10.3390/ma18122713.
38. Begines, B.; Alcudia, A.; Aguilera-Velazquez, R.; Martinez, G.; He, Y.; Trindade, G.F.; Wildman, R.; Sayagues, M.-J.; Jimenez-Ruiz, A.; Prado-Gotor, R. Design of Highly Stabilized Nanocomposite Inks Based on Biodegradable Polymer-Matrix and Gold Nanoparticles for Inkjet Printing. *Sci. Rep.* **2019**, *9*, 16097, doi:10.1038/s41598-019-52314-2.
39. Alshatnawi, F.; Alhendi, M.; Abbara, E.M.; Sivasubramony, R.; Garakani, B.; Enakerakpo, E.; Shaddock, D.; Stoffel, N.; Hoel, C.; Poliks, M.D.; et al. Electrical and Mechanical Behavior of Aerosol Jet–Printed Gold on Alumina Substrate for High-Temperature Applications. *Adv. Eng. Mater.* **2023**, *25*, 2300439, doi:10.1002/adem.202300439.
40. Jäger, J.; Schwenck, A.; Walter, D.; Bülau, A.; Gläser, K.; Zimmermann, A. Inkjet-Printed Temperature Sensors Characterized According to Standards. *Sensors* **2022**, *22*, 8145, doi:10.3390/s22218145.